

Inhibition of Aggregation of Amyloid Peptides by Beta-Sheet Breaker Peptides and Their Binding Affinity

Man Hoang Viet,[†] Son Tung Ngo,[‡] Nguyen Sy Lam,[§] and Mai Suan Li^{*,†}

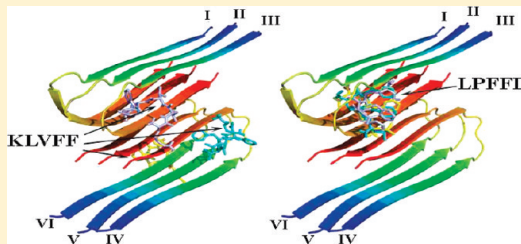
[†]Institute of Physics, Polish Academy of Sciences, Aleja Lotników 32/46, 02-668 Warsaw, Poland

[‡]Institute for Computational Science and Technology, 6 Quarter, Linh Trung Ward, Thu Duc District, Ho Chi Minh City, Vietnam

[§]Computational Physics Laboratory, Vietnam National University, Ho Chi Minh City, 227 Nguyen Van Cu, District 5, Vietnam

Supporting Information

ABSTRACT: The effects of beta-sheet breaker peptides KLVFF and LPFFD on the oligomerization of amyloid peptides were studied by all-atom simulations. It was found that LPFFD interferes the aggregation of $\text{A}\beta_{16-22}$ peptides to a greater extent than does KLVFF. Using the molecular mechanics-Poisson-Boltzmann surface area (MM-PBSA) method, we found that the former binds more strongly to $\text{A}\beta_{16-22}$. Therefore, by simulations, we have clarified the relationship between aggregation rates and binding affinity: the stronger the ligand binding, the slower the oligomerization process. The binding affinity of pentapeptides to full-length peptide $\text{A}\beta_{1-40}$ and its mature fibrils has been considered using the Autodock and MM-PBSA methods. The hydrophobic interaction between ligands and receptors plays a more important role for association than does hydrogen bonding. The influence of beta-sheet breaker peptides on the secondary structures of monomer $\text{A}\beta_{1-40}$ was studied in detail, and it turns out that, in their presence, the total beta-sheet content can be enhanced. However, the aggregation can be slowed because the beta-content is reduced in fibril-prone regions. Both pentapeptides strongly bind to monomer $\text{A}\beta_{1-40}$, as well as to mature fibrils, but KLVFF displays a lower binding affinity than LPFFD. Our findings are in accord with earlier experiments that both of these peptides can serve as prominent inhibitors. In addition, we predict that LPFFD inhibits/degrades the fibrillogenesis of full-length amyloid peptides better than KLVFF. This is probably related to a difference in their total hydrophobicities in that the higher the hydrophobicity, the lower the inhibitory capacity. The GROMOS96 43a1 force field with explicit water and the force field proposed by Morris et al. (Morris et al. *J. Comput. Chem.* 1998, 19, 1639) were employed for all-atom molecular dynamics simulations and Autodock experiments, respectively.



INTRODUCTION

Alzheimer's disease (AD) is the most common form of dementia among the senior population and is characterized pathologically by the progressive intracerebral accumulation of β -amyloid ($\text{A}\beta$) peptides. These peptides are proteolytic by-products of the $\text{A}\beta$ protein precursor and are most commonly composed of 40 ($\text{A}\beta_{1-40}$) and 42 ($\text{A}\beta_{1-42}$) amino acids. $\text{A}\beta$ peptides appear to be unstructured in their monomer state but aggregate to form fibrils with an ordered cross- β -sheet pattern.^{1–4} Increasing evidence from recent studies indicates that both soluble oligomers and mature fibrils are the toxic agents.^{5–7}

Presently, there is no cure or treatment for AD, and significant effort has, therefore, been made to find drugs to cope with this disease. One of the promising approaches is to inhibit and reverse misfolding and aggregation of amyloid peptides. To this end, a large number of potential $\text{A}\beta$ fibrillogenesis inhibitors have been proposed, such as carbohydrate-containing compounds,^{8,9} polyamines,^{10,11} chaperones,¹² metal chelators,¹³ osmolytes,¹⁴ and RNA aptamers¹⁵ (see also recent reviews^{16,17}). Nutraceuticals, which are natural products or extracts therefrom, as shown

by preclinical and certain clinical studies, might be of value as AD therapeutic agents.^{18,19}

The effect of N-methylated $\text{A}\beta_{16-22}$ peptide on the early steps of $\text{A}\beta_{16-22}$ fibril disassembly^{20,21} was theoretically studied by coarse-grained implicit-solvent molecular dynamics (MD) simulations.²² The binding of N-methylated $\text{A}\beta_{16-20}$ peptide to ordered $\text{A}\beta_{16-22}$ aggregates has also been considered by all-atom MD simulations with explicit solvent.²³ It has been shown that N-methylated peptides accelerate the degradation of $\text{A}\beta_{16-22}$ fibrils.

Because $\text{A}\beta$ is self-assembling, one possible strategy to prevent this process is to use short peptide fragments homologous to the full-length wild-type protein as inhibitors.^{24–29} Tjernberg et al. identified $\text{A}\beta_{16-20}$ (KLVFF), which binds to full-length $\text{A}\beta$ and prevents assembly into fibrils.²⁴ Soto and co-workers showed that the fragment $\text{A}\beta_{17-21}$ (LVFFA) does not display a high capacity to inhibit $\text{A}\beta$ fibrillogenesis, but peptide LPFFD

Received: December 8, 2010

Revised: April 22, 2011

Published: May 12, 2011

obtained from this fragment by proline replacement V18P and mutation A21D considerably enhances it.^{25,30}

The mechanism for LPFFD inhibiting the formation of β -sheet conformation of $A\beta_{1-42}$ was explored³¹ by the all-atom model with the GROMOS96 43a1 force field.³² The focus in that work was on the behavior of the salt bridge D23–K28, which plays the important role in stabilization of the turn region. This bridge is not stable, as the salt-bridge-forming atoms are solvated,³³ but if one makes it stable by forming a bond, the loop will be stable and will assist the peptide in forming a hairpin-like structure leading to acceleration of the fibril formation process. In fact, a recent experiment³⁴ showed that the aggregation rate of $A\beta_{1-40}$ -lactam[D23–K28], in which the residues D23 and K28 are chemically constrained by a lactam bridge, is nearly a 1000 times greater than in the wild-type. On the other hand, LPFFD was found to increase distance between D23 and K28 that form the salt bridge,³¹ and based on this fact, it was suggested that LPFFD interferes with aggregation by breaking the lactam bridge.³¹ The effect of KLVFF on the folding of monomer $A\beta_{1-40}$ and its aggregation has not yet been studied. Moreover, it remains unclear whether KLVFF or LPFFD is more efficient in preventing $A\beta$ aggregation and degrading fibrils.

A number of reasons also motivated us to theoretically study effects of KLVFF and LPFFD on $A\beta$ aggregation. It seems that the stronger the ligand binding to monomer or fibrils, the better the inhibition. However, despite much computational effort,^{22,23,35} there is no direct theoretical verification for this relationship. Another interesting problem is that the overall hydrophobicity of the ligands is more relevant to cytotoxicity than the amino acid sequence.³⁶ Because the total hydrophobicities of KLVFF and LPFFD are different, they can serve as good choices for studying the relationship between hydrophobicity and binding affinity. Thus, one of our goals is to study their influence on the aggregation of $A\beta$ peptides and their binding affinity. This should shed light on the correlation among binding, hydrophobicity, and aggregation kinetics.

Because the estimation of fibril assembly rates of full-length $A\beta$ peptides is computationally prohibitive, we chose the $A\beta_{16-22}$ fragment (KLVFFAE) for a model study. Using the GROMOS96 43a1 force field³² with explicit water, we showed that LPFFD slows the oligomerization of $A\beta_{16-22}$ to a greater extent than does KLVFF. Because the binding free energy of LPFFD to $A\beta_{16-22}$ obtained by the molecular mechanics–Poisson–Boltzmann surface area (MM-PBSA) method^{37,38} is lower than that for KLVFF, our results probably provide the first theoretical support for a correlation between the binding affinity and inhibitory ability: the stronger the binding, the slower the oligomerization process. Our findings also suggest that KLVFF is a more prominent inhibitor because of its lower total hydrophobicity compared to the LPFFD.

It is well-known that $A\beta_{1-42}$ peptides aggregate into β -sheet fibrils much faster than do $A\beta_{1-40}$ peptides.^{39–41} This pronounced difference is presumably due to the higher beta-content (β -content) in the monomer state of the former.^{42,43} Based on this fact, a strategy has been proposed for designing drugs to cope with Alzheimer's disease⁴³ in which ligands destabilizing the β -sheet monomer state would block the formation of neurotoxic oligomers. Then, an interesting question emerges as to whether this hypothesis remains valid in the presence of inhibitor/ligand. To answer this question, we performed conventional 300-ns MD simulations of monomer $A\beta_{1-40}$ and the two complexes $A\beta_{1-40} +$ KLVFF and $A\beta_{1-40} +$ LPFFD. To our surprise, neither beta-sheet

breaker reduces the total β -content of $A\beta_{1-40}$, but the prominent inhibitor LPFFD even enhances it. A more detailed analysis shows that they do decrease the β -content in fibril-prone regions. Thus, in the presence of a ligand, the correlation between the fibril formation rate and the β -content of the monomer state might no longer be valid. Instead, the inhibitory capacity of ligands is reflected in a reduction of the β -content in the fibril-prone regions. On the other hand, we have shown that inhibitors enhance the stability of $A\beta_{1-40}$. From this perspective, in the presence of ligand, the stability of the monomer state is a better indicator for fibrillogenesis than the total amount of β -content.

The susceptibility of two inhibitors to $A\beta_{1-40}$ and its mature fibrils has been studied in detail. For mature fibrils, we considered both 2-fold³ and 3-fold⁴⁴ structures. The results followed from the Autodock⁴⁵ and MM-PBSA methods show that LPFFD displays a higher binding affinity than KLVFF. This result suggests that the former degrades amyloid aggregates to a greater extent than the latter.

In short, in this article, we present three main results. First, LPFFD interferes with the oligomerization of $A\beta_{16-22}$ better than does KLVFF, and this is probably related to the difference in their binding affinities and hydrophobicities. Second, the capacity of blocking aggregation of $A\beta_{1-40}$ peptides is correlated with binding affinity but might not be associated with the reduction of the total β -content in the monomer state of the receptors. Therefore, studying ligand binding is a safe way to search for new leads in the drug-design problem. Third, our findings on the binding free energies of KLVFF and LPFFD to $A\beta_{1-40}$ and mature fibrils are compatible with experimental evidence^{24,25,30} that they inhibit aggregation of $A\beta$.

MATERIALS AND METHODS

Crystal Structures of Amyloid Peptides and Their Fibrils. In the Protein Data Bank (PDB), three possible structures with PDB codes 1BA6,⁴⁶ 1AML,⁴⁷ and 1BA4⁴⁸ are available for full-length $A\beta_{1-40}$. The structure 1BA6 is not considered because it is a methionine-oxidized form of $A\beta_{1-40}$.⁴⁶ Because this peptide is highly aggregation-prone in water, both structures 1AML and 1BA4 have been obtained in the water–micelle environment with pH values equal to 2.8 and 5.1, respectively.^{47,48} 1AML contains two helices (residues 15–23 and 31–35), whereas 1BA4 has one long helix expanded between residues 15 and 36. We chose 1BA4 for simulations because it was resolved in an environment with a pH closer to the pH of water.

Thus, the crystal structure of full-length $A\beta_{1-40}$ with PDB code 1BA4⁴⁸ was used in our simulations and docking experiments. The structures of monomers $A\beta_{16-22}$ (KLVFFAE) and $A\beta_{16-20}$ (KLVFF) were extracted from the structure of $A\beta_{10-35}$ peptide (PDB code 1hz3). The peptide LPFFD was derived from residues 17–21 of $A\beta_{10-35}$ with mutations V18P and A21D.²⁵

Because eight amino acids of the N-terminus of $A\beta_{1-40}$ are disordered in the fibril state, we neglected these amino acids in the construction of fibrils. We docked KLVFF and LPFFD to 2-fold-symmetric fibrils of six (6 $A\beta_{9-40}$) and 12 (12 $A\beta_{9-40}$) $A\beta_{9-40}$ peptides⁵⁰ and 3-fold symmetric fibrils of nine (9 $A\beta_{9-40}$) and 18 (18 $A\beta_{9-40}$) $A\beta_{9-40}$ chains.⁴⁴ The corresponding structures were kindly provided by Dr. R. Tycko.

Docking. To dock pentapeptides to full-length $A\beta$ peptides and their fibrils, we prepared a PDBQT file for the receptor and ligand using AutodockTools 1.5.4.⁴⁵ Autodock Vina, version

Table 1. Durations (in ns) of MD Runs Generated in Simulations

| trajectory | $\text{A}\beta_{16-22} + \text{KLVFF}$ | $\text{A}\beta_{16-22} + \text{LPFFD}$ | $2\text{A}\beta_{16-22}$ | $2\text{A}\beta_{16-22} + \text{KLVFF}$ | $2\text{A}\beta_{16-22} + \text{LPFFD}$ | $\text{A}\beta_{1-40}$ | $\text{A}\beta_{1-40} + \text{KLVFF}$ | $\text{A}\beta_{1-40} + \text{LPFFD}$ | $\text{A}\beta_{1-42}$ |
|------------|--|--|--------------------------|---|---|------------------------|---------------------------------------|---------------------------------------|------------------------|
| 1 | 200 | 200 | 144 | 560 | 338 | 300 | 300 | 300 | 300 |
| 2 | | | 149 | 600 | 409 | | | | |
| 3 | | | 179 | 340 | 325 | | | | |
| 4 | | | 175 | 282 | 338 | | | | |

1.1,⁵¹ which is much more efficient than Autodock 4, was employed. To describe atomic interactions, a modified version of the CHARMM force field was implemented.^{52,53} In the Autodock Vina software, the Broyden–Fletcher–Goldfarb–Shanno method⁵⁴ was employed for local optimization. To obtain reliable results, the exhaustiveness of the global search was set equal 400, and the maximum energy difference between the best binding mode and the worst one was chosen to be 7. Twenty binding modes (20 modes of docking) were generated with random starting positions of the ligand, which had fully flexible torsion degrees of freedom. The center of the grids was placed at the center of mass of the receptors, and the grid dimensions were $60 \times 40 \times 40$, $90 \times 70 \times 50$, and $50 \times 90 \times 90$ Å for $\text{A}\beta_{1-40}$, 2-fold-symmetric $6\text{A}\beta_{9-40}$ and 3-fold-symmetric $9\text{A}\beta_{9-40}$, respectively. For 2-fold-symmetric $12\text{A}\beta_{9-40}$ and 3-fold-symmetric $18\text{A}\beta_{9-40}$, grid dimensions of $100 \times 70 \times 70$ and $70 \times 100 \times 90$ Å, respectively, were used. These dimensions are large enough to cover the whole receptor.

MD Simulations. The GROMACS 4.0.5 package³² was used to run MD simulations with the GROMOS96 43a1 force field⁵⁵ and the SPC water model.⁵⁶ This force field has proved to be useful in studying aggregation of peptides (see, e.g., refs 57 and 58 and references therein). The equations of motion were integrated using a leapfrog algorithm⁵⁹ with a time step of 2 fs. The LINCS algorithm⁶⁰ was used to constrain the lengths of all covalent bonds with a relative geometrical tolerance of 10^{-4} . The V-rescale temperature coupling, which uses velocity rescaling with a stochastic term,⁶¹ was used to couple each system to the heat bath with a relaxation time of 0.1 ps. The Berendsen pressure coupling method⁶² was applied to describe the barostat with a constant pressure of 1 atm. The van der Waals (vdW) forces were calculated with a cutoff of 1.4 nm, and the particle–mesh Ewald method⁶³ was employed to treat the long-range electrostatic interactions. The nonbonded interaction pair list, with a cutoff of 1 nm, was updated every 10 fs.

The dimer of $\text{A}\beta_{16-22}$ ($2\text{A}\beta_{16-22}$) and the two complexes $2\text{A}\beta_{16-22} + \text{KLVFF}$ and $2\text{A}\beta_{16-22} + \text{LPFFD}$ were studied to probe the effects of inhibitors on oligomerization. For each of these systems, we performed four MD runs (trajectories) at $T = 300$ K. Initial conformations were generated by randomly placing the peptides in periodic boxes. The peptide concentrations of $\text{A}\beta_{16-22}$ and inhibitor were 67 and 33.5 nM, which are about 3 orders of magnitude higher than those used in experiments.²⁴

To estimate the binding free energies of the inhibitors to monomers $\text{A}\beta_{16-22}$ and $\text{A}\beta_{1-40}$ by the MM-PBSA method, we simulated the four systems $\text{A}\beta_{16-22} + \text{KLVFF}$, $\text{A}\beta_{16-22} + \text{LPFFD}$, $\text{A}\beta_{1-40} + \text{KLVFF}$, and $\text{A}\beta_{1-40} + \text{LPFFD}$. The durations of all MD runs are listed in Table 1. Because the durations of the runs were different, some remarks are in order. Because we are interested in thermodynamics of $\text{A}\beta_{16-22}$, $\text{A}\beta_{16-22} + \text{KLVFF}$, $\text{A}\beta_{16-22} + \text{LPFFD}$, $\text{A}\beta_{1-40}$, $\text{A}\beta_{1-40} + \text{KLVFF}$, $\text{A}\beta_{1-40} + \text{LPFFD}$, and $\text{A}\beta_{1-42}$, the corresponding MD runs should be

longer than times required to reach equilibrium (see below) and long enough to get good sampling. Therefore, MD runs of 200 and 300 ns were carried out for the first three systems and the last four systems, respectively (Table 1). One can show that these runs suffice for our purposes, as runs that were one-half as long (100 and 150 ns) provided the same results for the binding free energies.

In the cases of $2\text{A}\beta_{16-22}$, $2\text{A}\beta_{16-22} + \text{KLVFF}$, and $2\text{A}\beta_{16-22} + \text{LPFFD}$, we considered not only the thermodynamics but also the kinetics of fibril formation (see Figures 1–3 below). Therefore, the criterion for the lengths of the MD runs is that they should exceed fibril formation time $\tau_{\text{fib}}^{2A\beta}$ and be long enough for a reliable estimation of ΔG_{bind} . Trajectory 2 of $2\text{A}\beta_{16-22} + \text{LPFFD}$ (Figure 3) is the exception because the fibril-like state does not occur after 410 ns. We halted the MD run for this case when the order parameter P_2 remained low.

MM-PBSA Method. This section is available in the Supporting Information.

Tools and Measures Used in the Structure Analysis. Order Parameter P_2 . In characterizing the fibril-like states of short peptides, the nematic order parameter P_2 ^{57,64} is used. If P_2 is >0.5 , then a system has the propensity to be in an ordered state. In this article, we calculated P_2 for two peptides $\text{A}\beta_{16-22}$. The fibril-like state of these peptides has formed when one observes two antiparallel β -strands using visual molecular dynamics (VMD), and this was found to occur at $P_2 \approx 0.8$.

Contact Maps. The time evolutions of the formation of side-chain–side-chain (SC–SC) and hydrogen-bond (HB) contacts were monitored. An SC–SC contact was considered to be formed if the distance between the centers of mass of two residues was ≤ 6.5 Å. An HB was formed if the distance between donor D and acceptor A was ≤ 3.5 Å and the D–H–A angle was $\geq 135^\circ$.

Secondary Structures. To estimate secondary structures of monomer, $\text{A}\beta_{1-40}$ we used the definitions described earlier.^{65,66} Specifically, one assumes that, if dihedral angles ϕ and ψ are discretized into 20 intervals of 18° each, then β -strand conformations correspond to the vertices of the polygon $(-180^\circ, 180^\circ)$, $(-180^\circ, 126^\circ)$, $(-162^\circ, 126^\circ)$, $(-162^\circ, 108^\circ)$, $(-144^\circ, 108^\circ)$, $(-144^\circ, 90^\circ)$, $(-50^\circ, 90^\circ)$, and $(-50^\circ, 180^\circ)$ on the Ramachandran plot; the α helix structure is confined to the polygon $(-90^\circ, 0^\circ)$, $(-90^\circ, -54^\circ)$, $(-72^\circ, -54^\circ)$, $(-72^\circ, -72^\circ)$, $(-36^\circ, -72^\circ)$, $(-36^\circ, -18^\circ)$, $(-54^\circ, -18^\circ)$, and $(-54^\circ, 0^\circ)$. Other angles correspond to random coils. For dimer $2\text{A}\beta_{16-22}$, where HBs between the two peptides become important for monitoring fibril formation, we used the STRIDE algorithm^{67,68} because the definition of secondary structures in this algorithm is based not only on angles ϕ and ψ but also on HBs. From this perspective, STRIDE is more accurate than definitions based purely on geometrical constraints.

Free Energy Landscape. The free-energy surface along the N -dimensional reaction coordinate $V = (V_1, \dots, V_N)$ is given by $\Delta G(V) = -k_B T [\ln P(V) - \ln P_{\max}]$, where $P(V)$ is the

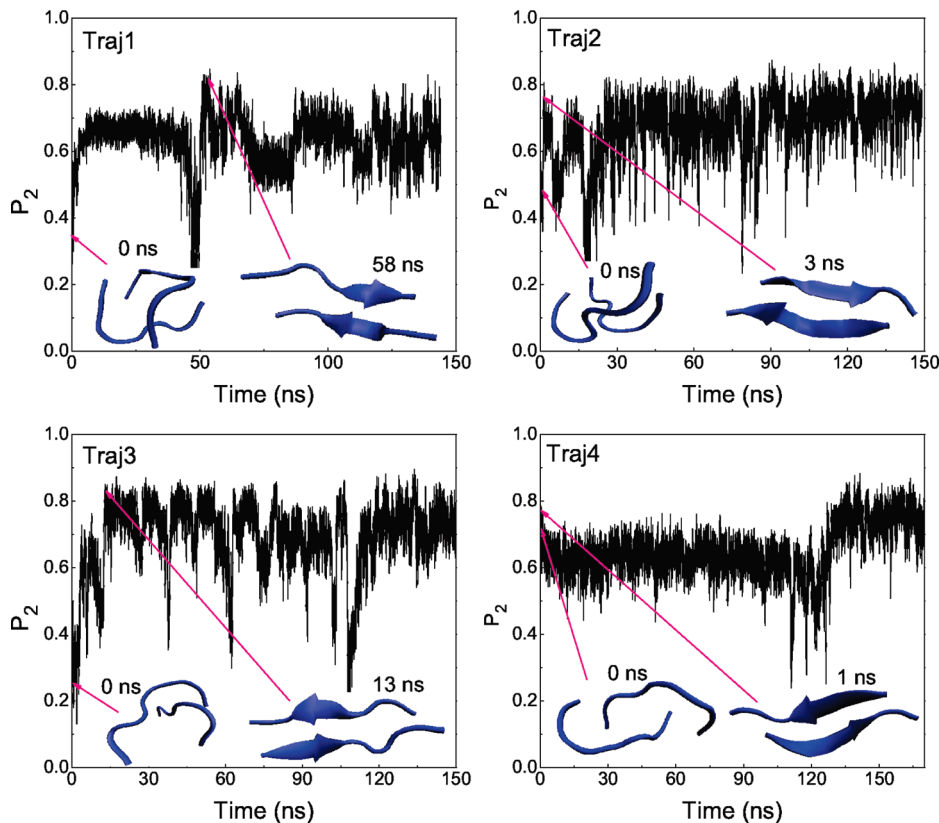


Figure 1. Time dependence of the order parameter P_2 for $2A\beta_{16-22}$ for four trajectories. Shown are initial and fibril-like snapshots. $\tau_{\text{fib}}^{2A\beta} \approx 58, 3, 13$, and 1 ns for the first, second, third, and fourth trajectories, respectively. The average value of fibril formation times is $\bar{\tau}_{\text{fib}}^{2A\beta} = 19 \pm 23$ ns.

probability distribution obtained from a histogram of MD data. P_{\max} is the maximum of the distribution, which is subtracted to ensure that $\Delta G = 0$ for the lowest-free-energy minimum. We used either helix content or β -content as the reaction coordinate for the one-dimensional free energy landscape (FEL). The helix-content (α -content) and the gyration radius (R_g) were also employed as reaction coordinates for the two-dimensional FEL.

RESULTS AND DISCUSSION

LPFFD Is More Efficient than KLVFF in Inhibition of Oligomerization of Dimer $2A\beta_{16-22}$. Dimer $2A\beta_{16-22}$. Because monitoring fibril formation of full-length amyloid peptides by all-atom simulations is beyond present computational capabilities, we considered the much shorter fragment $A\beta_{16-22}$. For illustration purposes, we studied the effects of KLVFF and LPFFD on this fragment. In the absence of pentapeptides, the fibril-like state of the dimer occurs rapidly in all four trajectories (Figure 1). The fastest ($\tau_{\text{fib}}^{2A\beta} \approx 1$ ns) and slowest ($\tau_{\text{fib}}^{2A\beta} \approx 58$ ns) fibril formations with two antiparallel $A\beta_{16-22}$ peptides were observed in the fourth and first MD runs, respectively. Averaging over four trajectories, we obtained the fibril formation time $\bar{\tau}_{\text{fib}}^{2A\beta} = 19 \pm 23$ ns. The fibril-like state in the fastest trajectory (trajectory 4) was highly unstable because it disappeared rapidly after formation at $\tau_{\text{fib}}^{2A\beta} \approx 1$ ns and did not occur again after more than 100 ns. Similarly to trajectory 2, in which the oligomerization was also fast, the route to the ordered state was not accompanied by intermediates, as no visible plateaus were observed in the time dependence of $P_2(t)$. This

behavior is in sharp contrast to that of trajectories 1 and 3, where relatively short-lived intermediates appeared (Figure 1).

$2A\beta_{16-22} + KLVFF$ System. The diversity of pathways to the ordered state of this system is shown in Figure 2. In the first trajectory, the antiparallel arrangement of one $A\beta_{16-22}$ and KLVFF occurred after ~ 18 ns. The fibril-like state of $2A\beta_{16-22}$ was observed at $\tau_{\text{fib}}^{2A\beta} \approx 20$ ns without intermediates. For this run, the ordered state for all three peptides did not appear. In the second MD run, the antiparallel ordering of two $A\beta_{16-22}$ peptides occurred at $\tau_{\text{fib}}^{2A\beta} \approx 56$ ns, but such an arrangement was not seen for the subsystem of one $A\beta_{16-22}$ and KLVFF. As in the first trajectory, the full ordering of three peptides was not observed. However, this kind of ordering occurs at relatively short time scales (about 150 ns) for trajectory 3 and 4 (Figure 2). The partial ordering of two peptides $A\beta_{16-22}$ appeared at $\tau_{\text{fib}}^{2A\beta} \approx 170$ and 122 ns for the third and fourth trajectories, respectively. Thus, the antiparallel arrangement of $2A\beta_{16-22}$ was observed in all four MD runs with the average time $\bar{\tau}_{\text{fib}}^{2A\beta} = 92 \pm 58$ ns. Because, within error bars, this value is not markedly higher than the $\bar{\tau}_{\text{fib}}^{2A\beta} = 19 \pm 23$ ns of the dimer case, it remains unclear whether peptide KLVFF slows the oligomerization of the $2A\beta_{16-22}$ system. However, because KLVFF considerably reduces the β -content of $2A\beta_{16-22}$ (see below), one can conclude that it interferes with fibril formation. From Figures 1 and 2, we obtained average values of P_2 equal to 0.72 and 0.61 for $2A\beta_{16-22}$ and $2A\beta_{16-22} + KLVFF$, respectively. These data further support KLVFF as an aggregation inhibitor.

$2A\beta_{16-22} + LPFFD$ Complex. As is evident from Figure 3, the antiparallel state of two peptides $A\beta_{16-22}$ occurred in the first MD run at $\tau_{\text{fib}}^{2A\beta} \approx 84$ ns. However, such a state was not observed

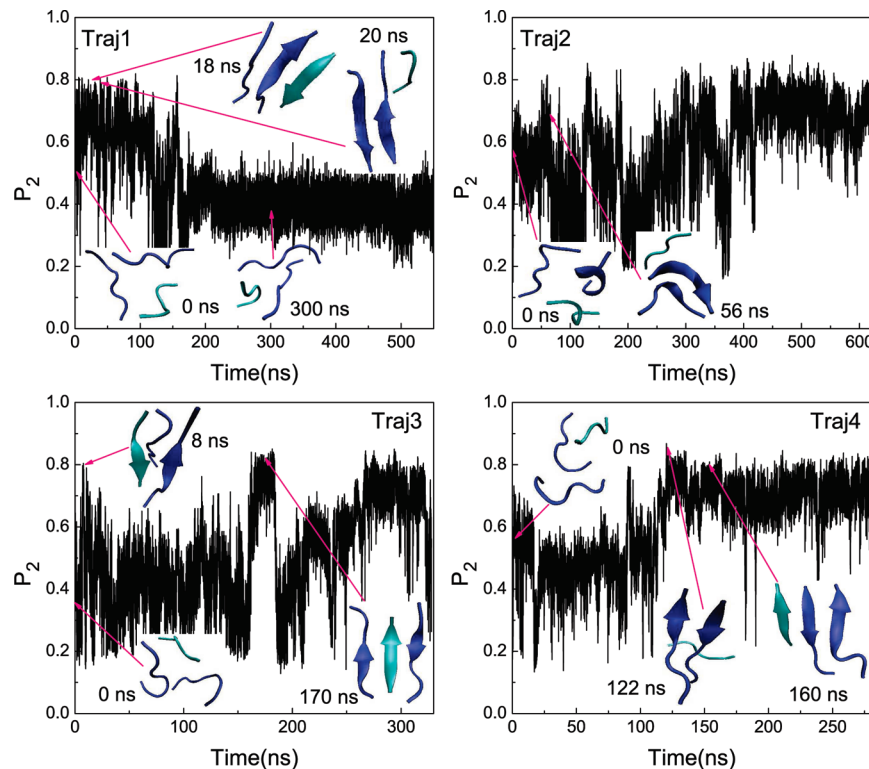


Figure 2. Time dependence of the order parameter P_2 for $2A\beta_{16-22} + KLVFF$ for four trajectories. The inhibitor KLVFF is shown in turquoise. $\tau_{fib}^{2A\beta} \approx 20, 56, 170$, and 122 ns for the first, second, third, and fourth trajectories, respectively. Averaging over four trajectories gives $\bar{\tau}_{fib}^{2A\beta} = 92 \pm 58$ ns.

in the second trajectory, implying that $\tau_{fib}^{2A\beta}$ should exceed its duration, 400 ns. The existence of several long-lived plateaus implies that intermediate states are necessary on routes to the ordered state of $2A\beta_{16-22}$. These intermediates were more pronounced compared to the case when beta-sheet breaker peptides were not present (Figure 1). One $A\beta_{16-22}$ peptide and LPFFD became antiparallel after about 304 and 51 ns for trajectories 2 and 4, respectively (Figure 3).

The antiparallel ordering of $2A\beta_{16-22}$ occurred in the third and fourth trajectories (Figure 3) at $\tau_{fib}^{2A\beta} \approx 17$ and 159 ns, respectively. The fast fibril formation in MD run 3 was not accompanied by long-lived intermediates, but such states did occur in the last run. Because the fibril-like state was not observed in the second trajectory, we obtained $\bar{\tau}_{fib}^{2A\beta} > 168$ ns, which is higher than the value for the KLVFF case. The difference in inhibitory capacities of the two beta-sheet breakers is even more obvious from the time dependence of the average β -contents of the $A\beta_{16-22}$ peptides (Figures S1–S3, Supporting Information). In the absence of inhibitors, the probability of being in beta-rich conformations was very high except for the first 50 ns in the first run (Figure S1, Supporting Information). KLVFF reduced the β -content of subsystem $2A\beta_{16-22}$ (Figure S2, Supporting Information) but to a much lesser extent compared to LPFFD (Figure S3, Supporting Information). The first and second trajectories in Figure S3 (Supporting Information), where the β -contents were reduced substantially, are the best examples of the inhibitory capacity of this peptide. Using the four trajectories shown in Figures S1–S3 (Supporting Information), one can determine average beta-sheet percentages of 57.52%, 32.98%, and 24.55% for $2A\beta_{16-22}$, $2A\beta_{16-22} + KLVFF$, and $2A\beta_{16-22} + LPFFD$, respectively. These results support not only the

inhibition effects of the two peptides but also the stronger interference of the oligomerization of $2A\beta_{16-22}$ by LPFFD than by KLVFF.

Binding Free Energies of LPFFD and KLVFF to $A\beta_{16-22}$ and $2A\beta_{16-22}$. To obtain the binding free energy, ΔG_{bind} , of beta-sheet breaker peptides to monomer $A\beta_{16-22}$ by the MM-PBSA method, we performed MD runs of 200 ns. As is evident from the time dependence of the interaction energy between two peptides, both systems $A\beta_{16-22} + KLVFF$ and $\beta_{16-22} + LPFFD$ reached equilibrium at time scales of 15 ns (Figure S4, Supporting Information). Note that the interaction energy, which involves electrostatic and van der Waals contributions, was computed without a cutoff (see also the Supporting Information). Only snapshots collected at equilibrium were used for the estimation. The results reported in Table 2 imply that LPFFD displays a higher binding affinity than KLVFF. This conclusion is in accord with the fact that the interaction energy of the former with $A\beta_{16-22}$ fluctuates to a lesser extent than that for the latter (Figure S4, Supporting Information). In both systems, the electrostatic interaction dominates over the vDW one. The large negative contributions of the Coulomb interaction are compensated by the polar terms (Table 2).

The binding free energies of pentapeptides to the dimer $2A\beta_{16-22}$ were estimated by the MM-PBSA method using snapshots generated in four trajectories for the $2A\beta_{16-22} + KLVFF$ and $2\beta_{16-22} + LPFFD$ systems (see Figures 2 and 3). Overall, equilibrium was reached after about 30 ns (Figure S5, Supporting Information) for all trajectories. The nature of binding remains the same as in the case of binding to monomer $A\beta_{16-22}$, that is, the vDW contribution is minor compared to the electrostatic one (Table 2). Within the error bars, the binding

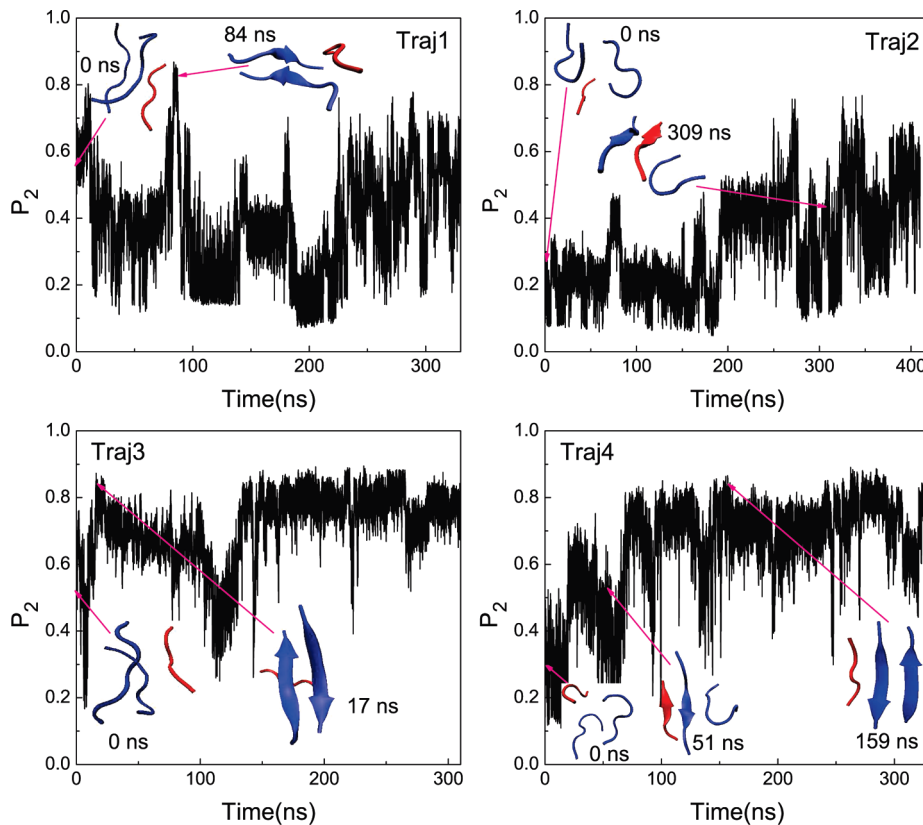


Figure 3. Time dependence of the order parameter P_2 for $2A\beta_{16-22} + \text{LPFFD}$ for four trajectories. The inhibitor LPFFD is colored in red. $\tau_{\text{fib}}^{2A\beta} \approx 84$, 17, and 159 ns for the first, third, and fourth trajectories, respectively. Because the fibril-like state of $2A\beta_{16-22}$ was not seen in the second run of 410 ns, we have $\tau_{\text{fib}}^{2A\beta} > 168$ ns.

Table 2. Binding Free Energies (in kcal/mol) of Pentapeptides to $A\beta_{16-22}$, $2A\beta_{16-22}$, and $A\beta_{1-40}$ Obtained by the MM-PBSA Method^a

| | ΔE_{elec} | ΔE_{vdW} | ΔG_{sur} | ΔG_{PB} | $-T\Delta S$ | ΔG_{bind} |
|----------------------------------|--------------------------|-------------------------|-------------------------|------------------------|----------------|--------------------------|
| $A\beta_{16-22} + \text{KLVFF}$ | -194.2 | -29.0 | -4.6 | 212.2 | 18.3 | 2.7 |
| $A\beta_{16-22} + \text{LPFFD}$ | -254.4 | -27.0 | -4.0 | 266.0 | 16.1 | -3.3 |
| $2A\beta_{16-22} + \text{KLVFF}$ | -171.0 ± 15.2 | -31.8 ± 3.7 | -4.8 ± 0.39 | 179.1 ± 16.8 | 25.4 ± 2.8 | -3.0 ± 0.38 |
| $2A\beta_{16-22} + \text{LPFFD}$ | -154.3 ± 16.2 | -33.3 ± 4.2 | -4.7 ± 0.42 | 163.5 ± 17.9 | 23.9 ± 2.5 | -4.9 ± 0.41 |
| $A\beta_{1-40} + \text{KLVFF}$ | -161.7 | -41.2 | -5.8 | 168.0 | 33.6 | -7.1 |
| $A\beta_{1-40} + \text{LPFFD}$ | 7.4 | -52.0 | -6.2 | 4.0 | 33.7 | -13.1 |

^a For $2A\beta_{16-22}$, results were averaged over four MD runs.

free energy of LPFFD (-4.9 kcal/mol) is lower than that of KLVFF (-3.0 kcal/mol).

Relationship among Binding, Hydrophobicity, and Aggregation Rates. In this section, we attempt to gain insight into the interplay between the binding affinity, total ligand hydrophobicity, and oligomerization rates using the results obtained for the $A\beta_{16-22}$ systems. Because LPFFD is more susceptible to $A\beta_{16-22}$ and inhibits the oligomerization of $2A\beta_{16-22}$ to a greater extent than KLVFF, one might expect the correlation between binding affinity and inhibitory capacity to be that the tighter the binding, the stronger the inhibition effect. To the best of our knowledge, such a relationship has not previously been demonstrated on the quantitative level.

To strengthen the hypothesis about the relationship between binding affinity and inhibitory action, let us discuss other examples. Experimentally, it has been established that a commercially

available grape seed polyphenolic extract, MegaNatural-AZ (MN), inhibits $A\beta$ aggregation to a greater extent than does ligand NGA9-119 (NGA).⁶⁹ Using Autodock Vina, version 1.1,⁵¹ we have shown that MN, for instance, has a lower binding energy to 3-fold-symmetric $9A\beta_{9-40}$ ($E_{\text{bind}} = -10.4$ kcal/mol) than does NGA ($E_{\text{bind}} = -8.6$ kcal/mol) (D. T. Dung and M. S. Li, unpublished results). Thus, the experimental data of Ono et al.⁶⁹ and our theoretical result are consistent with the hypothesis proposed herein. Another example is that, in *in vitro* experiments,⁷⁰ Curcumin was found to inhibit the fibril formation of $A\beta_{1-40}$ to a greater extent than Naproxen and Ibuprofen. Using the MM-PBSA method^{37,38} and GROMOS96 43a1 force field,³² we found that, compared to the other two ligands, the binding energy of Curcumin to monomer $A\beta_{1-40}$ is lower. Specifically, $E_{\text{bind}} = -21.6$, -8.7 , and -5.5 kcal/mol for Curcumin, Naproxen, and Ibuprofen, respectively (S. T. Ngo and M. S.

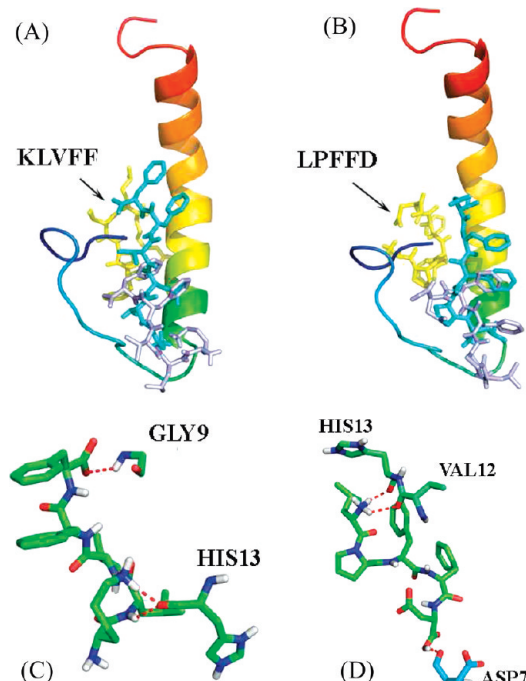


Figure 4. Binding sites of KLVFF and LPFFD to $\text{A}\beta_{1-40}$ peptide (mode 1, silver; mode 2, green; mode 3, yellow) and hydrogen bonds of the best mode (mode 1).

Li, unpublished results). Again these estimations support the hypothesis that tight binding would promote a strong inhibition effect, but more studies are needed for confirmation.

Using values of the individual hydrophobicities of amino acids,⁷¹ we obtained total hydrophobicities of $\text{Hyd}_{\text{total}} = -3.54$ and -4.89 kcal/mol for LPFFD and KLVFF, respectively. These values of $\text{Hyd}_{\text{total}}$ allow us to speculate that the strong blockage of aggregation by LPFFD comes from its lower hydrophobicity. Our suggestion is consistent with the experimental result²⁵ that, with $\text{Hyd}_{\text{total}} = -8.05 \text{ kcal/mol}$, LVFFA is much worse than LPFFD in interfering with the fibrillogenesis of full-length $\text{A}\beta$ peptides.

To substantiate our suggestion about the relationship between hydrophobicity and binding capacity, we designed several sequences that might be more efficient than LPFFD. For instance, using Autodock Vina, version 1.1,⁵¹ we found NHPFV and NQYYV to display higher binding affinities to $\text{A}\beta_{1-40}$ than LPFFD, with $E_{\text{bind}} = -6.7$ and -7.0 kcal/mol , respectively. These values clearly are lower than $E_{\text{bind}} = -6.3 \text{ kcal/mol}$ of LPFFD. Because NHPFV and NQYYV have $\text{Hyd}_{\text{total}} = -2.01$ and -1.03 , respectively, their dominance over LPFFD is consistent with the relationship proposed herein between inhibition and hydrophobicity. It should be noted that we have obtained only preliminary evidence for the correlation between inhibition, binding, and hydrophobicity. Many more studies are needed to clarify this important issue.

Binding of LPFFD and KLVFF to $\text{A}\beta_{1-40}$ Peptide. The results that we obtained for the short $\text{A}\beta_{16-22}$ peptide suggest that the binding affinity of pentapeptides is correlated with their inhibitory ability. Because the estimation of oligomerization rates of $\text{A}\beta_{1-40}$ by all-atom simulations is beyond present computational capabilities, to gain information about the influence of ligands on oligomerization, we restricted ourselves to calculating ΔG_{bind} using both the Autodock and MM-PBSA methods.

Table 3. Binding Energies (in kcal/mol) of Pentapeptides to $\text{A}\beta_{1-40}$ and Mature Fibrils as Obtained by the Docking Method

| | KLVFF | LPFFD |
|--|----------------|----------------|
| $\text{A}\beta_{1-40}$ (PDB code 1BA4) | -5.5 | -6.3 |
| $\text{A}\beta_{1-40}$ (259 clusters) | -4.9 ± 0.2 | -5.5 ± 0.2 |
| 2-fold $6\text{A}\beta_{9-40}$ | -6.7 | -7.1 |
| 3-fold $9\text{A}\beta_{9-40}$ | -7.0 | -9.0 |
| 2-fold $12\text{A}\beta_{9-40}$ | -6.2 | -6.9 |
| 3-fold $18\text{A}\beta_{9-40}$ | -6.7 | -8.3 |

Docking Result. We first docked pentapeptides to $\text{A}\beta_{1-40}$ using the structure taken from PDB (PDB code 1BA4⁴⁸). The three best modes (lowest energies) are shown in Figure 4. Both KLVFF and LPFFD are located near the N-terminal. In the best position, KLVFF is bound by three HBs with Gly9 and His13 of the receptor. LPFFD also forms three HBs not only with His13 but also with Asp7 and Val12. Although the HB networks are the same, this peptide docks to $\text{A}\beta_{1-40}$ with greater strength than does KLVFF because of the domination of the vdW interaction, as follows from the MM-PBSA analysis (Table 2). The corresponding binding energies are listed in Table 3. Because the structure of isolated $\text{A}\beta_{1-40}$ used for docking was resolved in a water–micelle environment,⁴⁸ our results were applied to this type of solution.

Because the structure of $\text{A}\beta_{1-40}$ in water is not yet known, to estimate the binding energy in this environment by docking, we employed the flexible receptor method.⁷² That is, we used the C_α rmsd conformational clustering method implemented in the GROMACS software and snapshots collected in a 300-ns MD run for monomer $\text{A}\beta_{1-40}$. With a clustering tolerance of 1.0 \AA , we obtained 259 representative structures that we used for docking. We obtained average (over 259 structures) values of $\Delta E_{\text{bind}} = -5.5 \pm 0.2$ and $-4.9 \pm 0.2 \text{ kcal/mol}$ for LPFFD and KLVFF, respectively. Thus, both the docking and MM-PBSA methods imply that KLVFF displays a lower binding affinity in aqueous solution.

MM-PBSA Results. Because the docking technique is not sufficiently accurate because of the omission of receptor dynamics and a limited number of trial positions of ligand, we also estimated ΔG_{bind} by the MM-PBSA method. The systems reached equilibrium after about 50 ns (Figure S6, Supporting Information), and only snapshots collected in the last 250 ns were used for estimation. The contribution of the electrostatic interaction to ΔG_{bind} of KLVFF is greater than the vdW contribution (Table 2). The situation becomes very different for the LPFFD case, where the vdW interaction between the ligand and receptor dominates over both the Coulomb and polar contributions. Such a dramatic difference presumably comes from the fact that the total charge of $\text{A}\beta_{1-40}$ is -3 , whereas KLVFF and LPFFD have charges equal to $+1$ and -1 , respectively [lysine (K) of KLVFF is positively charged, whereas the last aspartic acid (D) from LPFFD carries the negative charge]. This also partially explains why the Coulomb interaction between the receptor and LPFFD is repulsive (Table 2).

As mentioned in the Supporting Information, to estimate the vibrational entropy by normal-mode analysis, one has to minimize structures with no cutoff for nonbonded interactions in a vacuum. To this end, we first applied the conjugate gradient method and then used the Broyden–Fletcher–Goldfarb–Shanno method⁵⁴ to create better approximations of the inverse

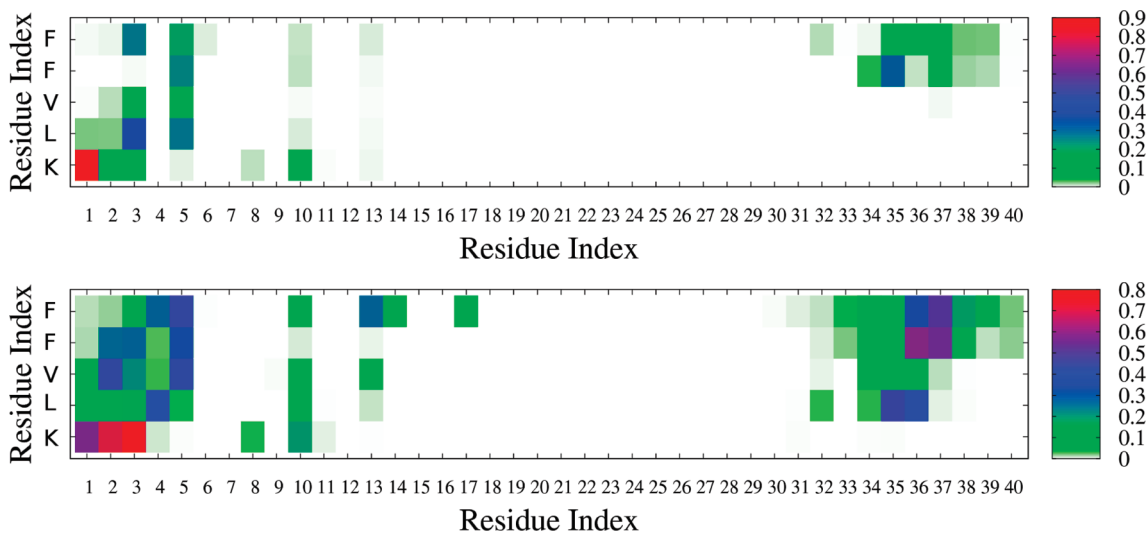


Figure 5. Hydrogen-bond (top) and side-chain (bottom) contact maps for KLVFF and $\text{A}\beta_{1-40}$. Results were obtained from the 300-ns run of MD simulation.

Hessian matrix, moving the system to the currently estimated minimum. In addition to the conjugate gradient method, we also used the steepest-descent method, but the post-minimization structures remained essentially the same, implying the convergence of our procedure. The estimation of the vibrational entropy is reliable because of the small rmsd between the pre- and post-minimization structures (rmsd ≈ 0.15 nm for $\text{A}\beta_{1-40}$). Such a small difference in structures is expected because $\text{A}\beta_{1-40}$ contains the hydrophobic core $\text{A}\beta_{16-22}$, which prevents the system from high exposure to solvent. On the other hand, water molecules are known to fluctuate around the backbone atoms and weaken HBs between amino acids.⁷³ Thus, in a vacuum, hydrogen bonding becomes stronger, keeping post-minimization structures close to pre-minimization ones.

The binding free energy of LPFFD to the receptor of $\Delta G_{\text{bind}} \approx -13.1$ kcal/mol is markedly lower than $\Delta G_{\text{bind}} \approx -7.1$ kcal/mol for KLVFF. This trend is consistent with the results obtained by the Autodock Vina version of docking (Table 3). Thus, both the docking and MM-PBSA approaches support the experimental fact that both peptides inhibit the fibril growth of $\text{A}\beta_{1-40}$. Moreover, we predict that LPFFD is more prominent than KLVFF.

Hydrophobic Interaction Is More Important than HB One. The main driving force for the binding process can be revealed by constructing HB and SC–SC contact maps (the criterion for contact formation is given in Material and Method). As follows from Figures 5 and 6, the hydrophobic interaction dominates over the HB one. This effect becomes even more pronounced in the case of LPFFD, which mainly locates around the C-terminus (Figure 6), whereas KLVFF visits the two termini with nearly the same probabilities (Figure 5). A more detailed binding picture can be obtained by calculating the distances between each pair of residues of the ligand and receptor (Figure S7, Supporting Information). Because the N-terminus is not relevant to fibril formation,^{3,50,74} the high probability of pentapeptide location near the fibril-prone C-terminus is in accord with the fact that LPFFD is more efficient than KLVFF. Phe²⁰ and Lys¹⁶ of KLVFF show the highest susceptibilities to the C- and N-termini, respectively, whereas Leu¹⁷ exhibits stronger binding to residues 10–17 than the remaining residues (Figure S7, Supporting

Information). This observation is in line with the experimental fact that these three amino acids are critical for binding of KLVFF to $\text{A}\beta_{1-40}$ and inhibition of fibril formation.²⁴ Finally, as is evident from Figure 5, KLVFF spends very little time near amino acids 16–20. Thus, it is not expected to bind to the homologous sequence in the monomer $\text{A}\beta_{1-40}$ peptide.

Effect of Beta-Sheet Breaker Peptides on Secondary Structures of $\text{A}\beta_{1-40}$. Monomer $\text{A}\beta_{1-40}$ Displays a Crossover from Helix to Random-Coil (RC) Conformation. It should be noted that $\text{A}\beta$ peptides have very high propensities to aggregation, and for this reason, it has not yet been possible to study the full-length peptides in water solution. In water but at low pH, fragments of $\text{A}\beta$ adopt mainly coil structures.^{75,76} To avoid aggregation, experiments have been performed in mixtures of water and organic solvents such as micellar solutions,^{48,77} trifluoroethanol,^{78,79} or hexafluoroisopropanol.^{80,81} Under these conditions, the full-length $\text{A}\beta$ peptides display substantial helical structure.

The time dependence of the beta, helix, and RC contents of $\text{A}\beta_{1-40}$ is shown in Figure 7. For single $\text{A}\beta_{1-40}$, these quantities are quite stable in the first 150 ns. From about 150 to 160 ns, a structural transition from helix-rich structures to RC-rich ones occurs. The existence of such a crossover is consistent with the weak two-state behavior (two local minima separated by a low barrier) of the free energy plotted as a function of α -content (Figure 8). The sudden increase in α -content is accompanied by a sharp drop of RC content. After the crossover, the helix and RC contents undergo little variations, but the β -content keeps changing, although no pronounced crossover in the β -content behavior is observed (Figure 7), reflecting the downhill FEL plotted as a function of the β -content (Figure S8, Supporting Information).

Our canonical MD simulations show that, at short time scales (≤ 150 ns), the monomer state of $\text{A}\beta_{1-40}$ is rich in α -content (Figure 7). The crossover to the low-helix-content region occurs at $150 \leq t \leq 160$ ns, where the increase in random-coil content is also observed. At larger time scales (≥ 160 ns), coil structures become dominant (Figure 7), and the average values of the beta, helix, and coil contents are equal to 11.8%, 32.1%, and 56.1%, respectively. If one considers secondary structures in equilibrium at $t \geq 50$ ns (Figure S6, Supporting Information), then the

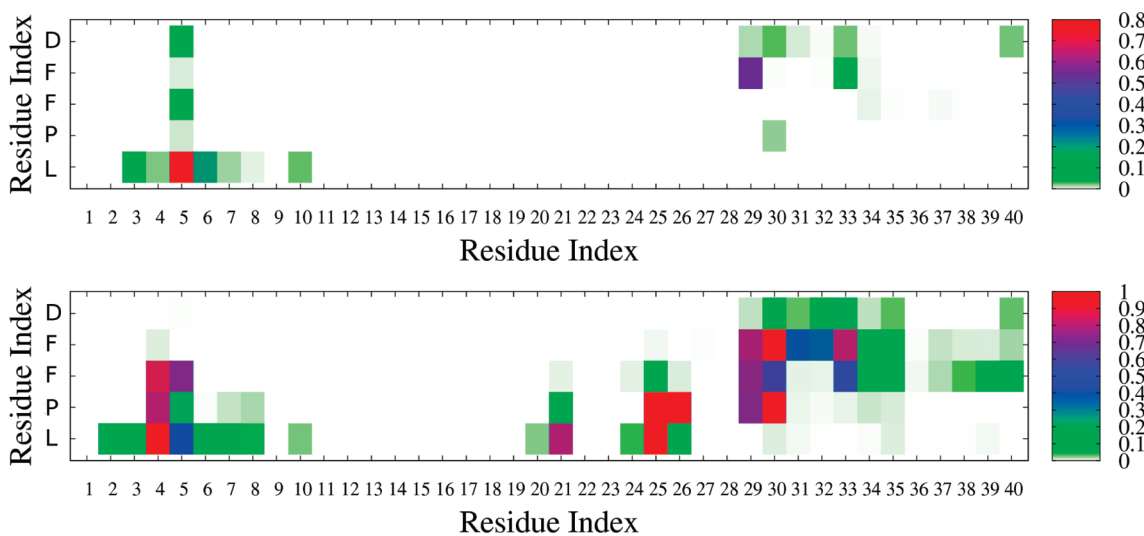


Figure 6. Hydrogen-bond (top) and side-chain (bottom) contact maps for LPFFD and $\text{A}\beta_{1-40}$. Results were obtained from the 300-ns run of MD simulation.

average values of the beta, helix, and coil fractions become 11.2%, 38.0%, and 50.8%, respectively. This implies that, in concert with the helix (or coil) crossover scenario, one observes changes (compared to equilibrium values) at large time scales for the helix and coil contents but not for the beta content. Because these changes are not so dramatic, we estimate the jump in helix and random coil contents as the difference between their average values before and after the crossover. Pre- and post-crossover average values were calculated by averaging over the time periods of 50–150 ns (the first 50 ns are skipped, as the system has not yet reached equilibrium yet) and 160–300 ns, respectively (Figure 7). We obtained the jump in α -content as $\Delta\alpha = 13.8\%$ and the jump in random-coil content as $\Delta\text{RC} = 12.6\%$. These values display notable differences in secondary structures between the two regimes.

Using the clustering technique with a tolerance of 3 Å C_α rmsd, we obtained three clusters with typical structures shown in Figure S9 (Supporting Information). Because the behavior of secondary structures remains stable over this sufficiently long period, one can expect that it holds for longer time scales. Therefore, our canonical 300-ns MD simulations suggest that, in water solution, the monomer state of $\text{A}\beta_{1-40}$ is mainly RC, but helix and beta structures are also present.

It seems that our simulations provide an α -content higher than that obtained from previous all-atom replica exchange simulations with explicit⁴² and implicit⁴³ water. Sgourakis et al. used Amber-derived PARM94, PARM96, MOD-PARM, GROMOS, and OPLS force fields, whereas the recently improved version of the Amber force field PARM99SB was employed by Yang and Teplow.⁴³ With the help of a coarse-grained model, Vitalis and Caflisch⁸² obtained a reasonable agreement with the CD estimates of 5% α -content and 25% β -content in aqueous buffer at 298 K.⁸³ This result is also different from ours. Our estimations agree with the results obtained with the UNRES force field,⁸⁴ which also favors helices. Thus, the problem of the intrinsic structure of monomer $\text{A}\beta_{1-40}$ in an aqueous environment remains open, requiring further investigation.

Inhibitors Wash out the Crossover from Helix to Random-Coil Conformation. The presence of inhibitors does not substantially change the time dependence of the β -content, but the

crossover from the helix to the RC state becomes much less pronounced (Figure 7). As a result, the FEL profile adopts a downhill shape (color curves in Figure 8) instead of a two-state one. The smeared crossover between helix-rich and RC-rich conformations appears at different time scales. Namely, the most appreciable change is observed at ~ 250 and ~ 40 ns for the $\text{A}\beta_{1-40} + \text{KLVFF}$ and $\text{A}\beta_{1-40} + \text{LPFFD}$ complexes, respectively (Figure 7).

LPFFD Enhances β -Content but Not in Fibril-Prone Regions. It is well-known that the fibril formation rates are strongly correlated with the population of the fibril-prone conformation in monomer state.^{58,85,86} Because the fibril-prone conformation of full-length amyloid peptides is rich in β -content, previous MD simulations⁴³ suggested that the larger enhancement of β -content at the C-terminal of monomer $\text{A}\beta_{1-42}$ compared to $\text{A}\beta_{1-40}$ is associated with the experimental fact that the former aggregates much faster than the latter one.^{39–41} Peptide KLVFF has a little effect on the overall beta structure while LPFFD enhances it substantially (Figures 7 and 9). This result would suggest that LPFFD accelerates the fibril formation of $\text{A}\beta_{1-40}$ but not slow it down as expected from experiments. The puzzle may be solved if one reminds that the β -content shown in Figure 7 is the total one. So to decide if pentapeptides can inhibit oligomerization one has to consider fibril-prone regions. KLVFF inhibits the fibril formation of $\text{A}\beta_{1-40}$ because it reduces the β -content of the last 28–40 amino acids (Figure 7b,a). LPFFD does not decrease the total amount of β -content in this region (Figure 7c,a) but in its presence fibril-prone amino acids 28–32 become unstructured. This is probably responsible for inhibitory ability of LPFFD. Thus, aggregation rates of $\text{A}\beta$ are correlated with the β -content of fibril-prone regions in the monomer state but not with the total one.

Effect of Proline in LPFFD as a Beta-Sheet Breaker. It is well-known that proline replacement can greatly reduce the propensity of the polypeptide chains for fibril formation.^{30,87} Herein, we analyze the role of proline in LPFFD in the inhibition of the fibrillogenesis of $\text{A}\beta_{1-40}$. As follows from Figure 6, proline strongly interacts with residues 4, 25, 26, 29, and 30. On the other hand, the β -content of these residues is essentially zero (Figure 9), implying that proline substantially suppresses it.

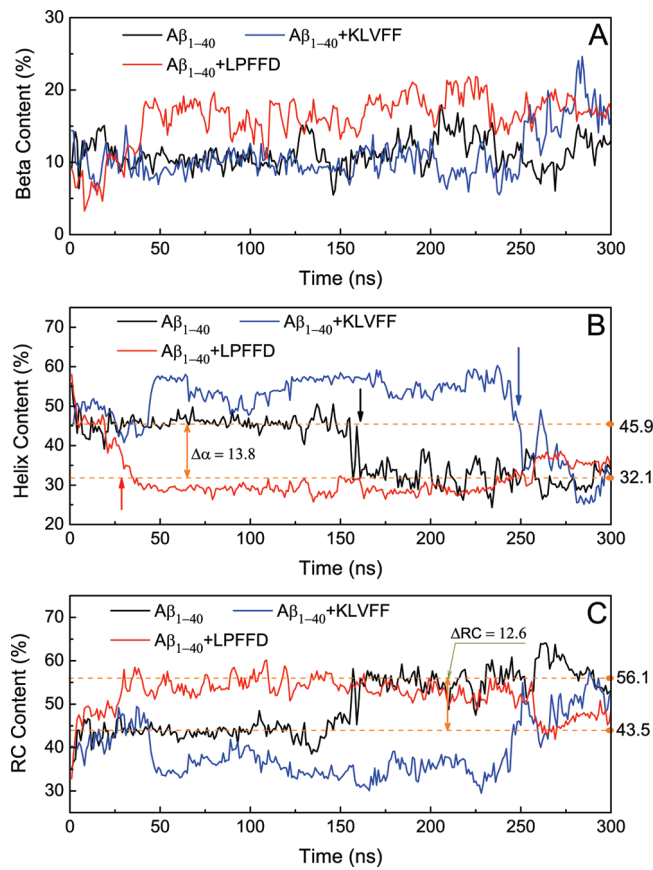


Figure 7. Time dependence of the secondary structure contents of $\text{A}\beta_{1-40}$ peptide in the $\text{A}\beta_{1-40}$ (black line), $\text{A}\beta_{1-40}$ with KLVFF (blue line), and $\text{A}\beta_{1-40}$ with LPFFD (red line) systems. Results were averaged every 1 ns. Arrows refer to times when the α -content undergoes a significant change. Upper and lower dotted lines in panel B refer to the average values of α -content during periods of 50–150 ns (before jump) and 160–300 ns (after jump). The average values of pre- and post-cross-over α -contents are 45.9% and 31.2%, respectively. Therefore, the jump between the two regimes is $\Delta\alpha = 13.8\%$. Lower and upper dotted lines in panel C refer to the average values of random-coil content during periods of 50–150 ns (before jump) and 160–300 ns (after jump). The average values of pre- and post-cross-over random-coil contents are 43.5% and 56.1%, respectively. The corresponding jump in random-coil content is $\Delta\text{RC} = 12.6\%$.

Because the affinity of peptides to form fibrillar structures depends on the beta-content in the fibril-prone regions of the monomer, one can expect that proline in LPFFD strongly reduces the propensity of $\text{A}\beta_{1-40}$ to self-assemble.

$\text{A}\beta_{1-40}$ Becomes More Stable in the Presence of Inhibitors. Because stable polypeptide chains show a low propensity for aggregation, one can gain information about the inhibition capabilities of beta-breaker peptides by studying their influence on the stability of the receptor. As is evident from Figure 10, the two-dimensional R_g – α -content FEL of monomer $\text{A}\beta_{1-40}$ has three basins, but in the presence of pentapeptides they shrink into a single one, suggesting that $\text{A}\beta_{1-40} + \text{KLVFF}$ and $\text{A}\beta_{1-40} + \text{LPFFD}$ are more stable than $\text{A}\beta_{1-40}$. This conclusion remains valid if one uses R_g and β -content as the reaction coordinates (Figure S10, Supporting Information), because, in the absence of the inhibitors, the single $\text{A}\beta_{1-40}$ FEL has one local basin more. Therefore, beta-sheet breakers should disfavor aggregation.

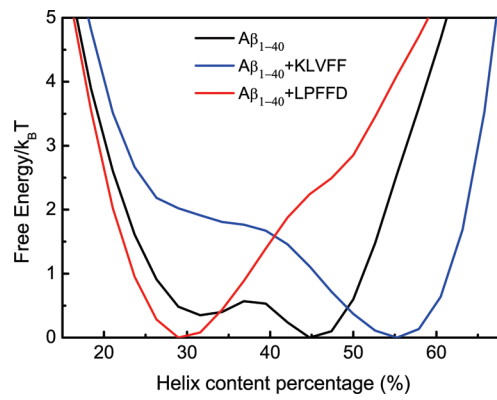


Figure 8. One-dimensional FELs of $\text{A}\beta_{1-40}$, $\text{A}\beta_{1-40} + \text{KLVFF}$, and $\text{A}\beta_{1-40} + \text{LPFFD}$, where the α -content is the reaction coordinate. Results obtained from the MD run of 300 ns.

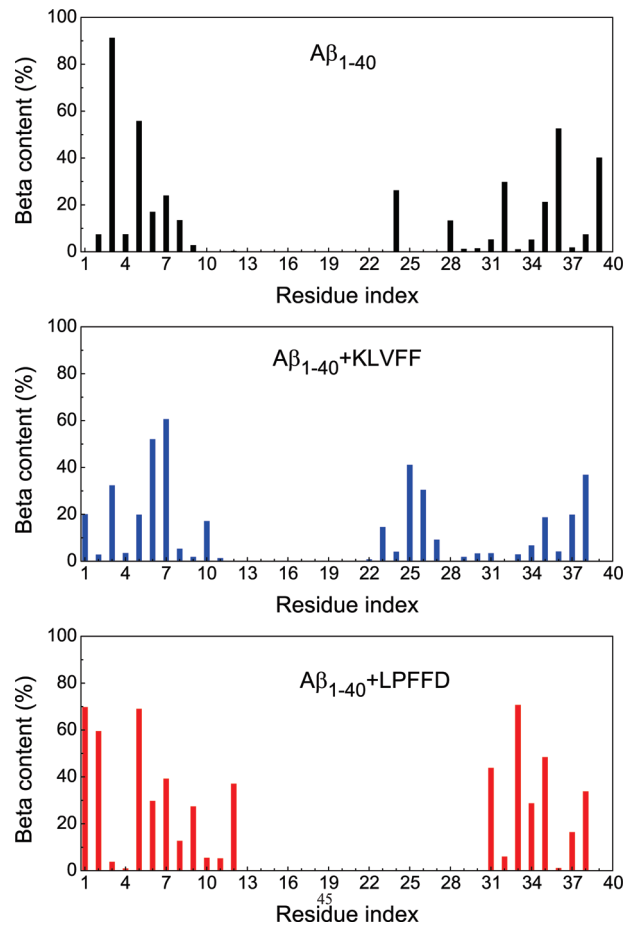


Figure 9. Population of β -content of each residue of $\text{A}\beta_{1-40}$ for the $\text{A}\beta_{1-40}$ (black), $\text{A}\beta_{1-40} + \text{KLVFF}$ (blue), and $\text{A}\beta_{1-40} + \text{LPFFD}$ (red) systems.

More importantly, the stability of the monomer state is a more unique measure for characterizing the fibrillogenesis of $\text{A}\beta$ peptides than the β -content.

Estimations of Binding Energies of Pentapeptides to Mature Fibrils by the Docking Method. Because mature fibrils are large systems, the calculation of ΔG_{bind} by the MM-PBSA

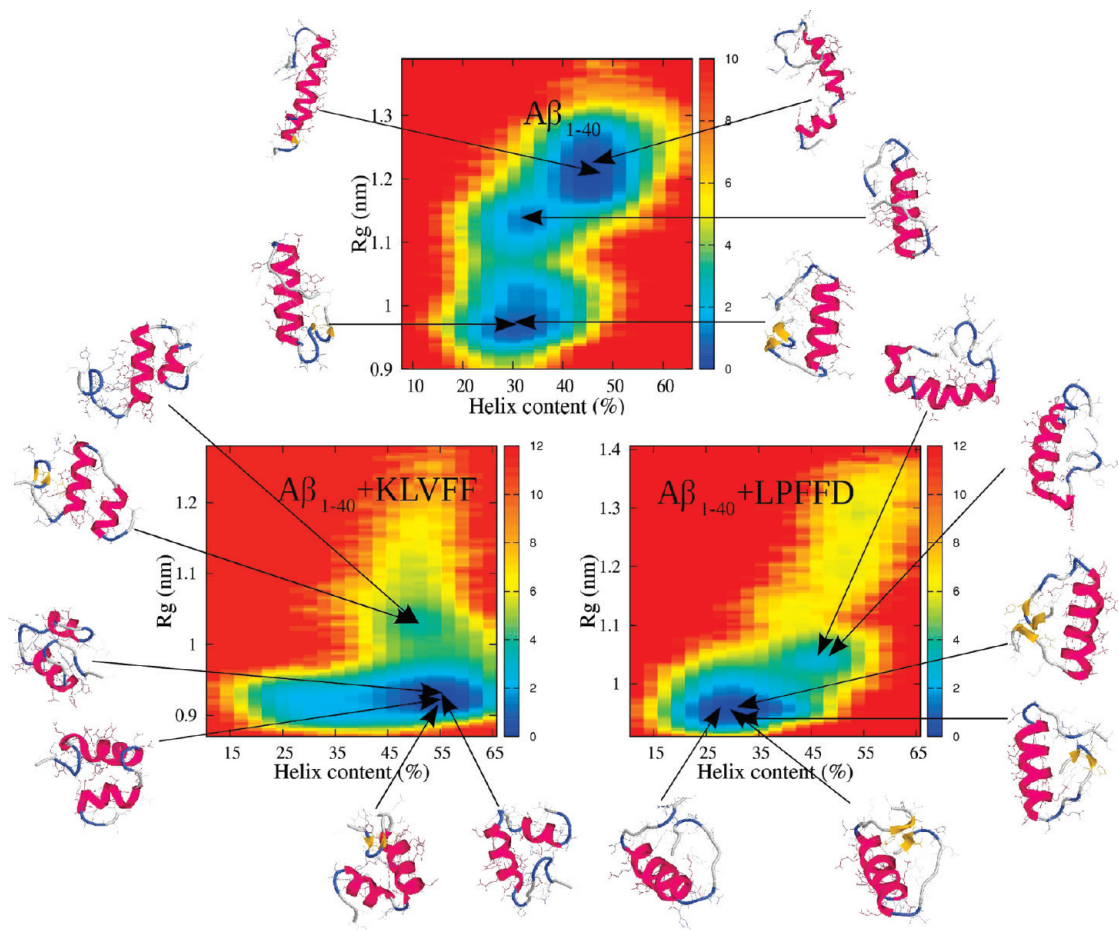


Figure 10. Two-dimentional FELs of $\text{A}\beta_{1-40}$, $\text{A}\beta_{1-40} + \text{KLVFF}$, and $\text{A}\beta_{1-40} + \text{LPFFD}$, plotted as a function of R_g and α -content. Results obtained from the MD run of 300 ns.

method is time-consuming, so we restrict ourselves to estimation of the binding energy by the docking approach.

Binding to 2-Fold-Symmetric $6\text{A}\beta_{9-40}$. We chose a system of two layers containing three $\text{A}\beta_{9-40}$ peptides each (Figure 11). Using Autodock Vina, version 1.1,⁵¹ we obtained ΔE_{bind} for KLVFF and LPFFD (Table 3). For the best mode with the lowest binding energy, both inhibitors are located inside the receptor, but their positions are different. Peptide KLVFF is bound to peptide II from the upper layer of $6\text{A}\beta_{9-40}$ by two HBs with Asp15 (II) and Ala22 (II). LPFFD shows a higher binding affinity (Table 3) than KLVFF, having one additional HB (Figure 11). This is because, contrary to KLVFF, which binds to a single $\text{A}\beta_{9-40}$ peptide II, LPFFD is also docked to peptide III.

The difference in binding capacity of the two pentapeptides can be obtained by monitoring the number of SC contacts between ligand and receptor. K, L, V, F, and F of KLVFF form two, one, two, two, and five contacts, respectively, with chain VI of $6\text{A}\beta_{9-40}$ (Figure 11). The last residue F also has one contact with Glu23 of chain IV. Thus, in the best docking mode, this pentapeptide forms 13 SC contacts with receptor chain VI that display the strongest binding. LPFFD also shows very tight binding to chain VI through SC contacts. Specifically, residues L, P, F, F, and D have three, one, one, three, and five contacts, respectively, with this chain. In addition, two SC contacts with chain IV are formed by amino acids L and P. In total, LPFFD has

15 SC contacts with $6\text{A}\beta_{9-40}$. Because this number of contacts is larger than that of KLVFF, LPFFD has a lower E_{bind} value.

Binding to 3-Fold-Symmetric $9\text{A}\beta_{9-40}$. The 3-fold-symmetric structure of $9\text{A}\beta_{9-40}$, resolved by Paravastu et al.,⁴⁴ is shown in Figure 12. For the three lowest modes, peptide KLVFF docks to three different corners. In the best mode, it has four HBs with peptide VII from the $9\text{A}\beta_{9-40}$ complex, and the corresponding binding energy is $E_{\text{bind}} \approx -7.0$ kcal/mol (Table 3). Peptide LPFFD displays strong binding to the receptor, forming seven HBs with peptides I, II, VII, VIII, and IX from two different patches (each patch contains three parallel $\text{A}\beta_{9-40}$ peptides). This strong HB network gives rise to a low binding energy of $\Delta E_{\text{bind}} \approx -9.0$ kcal/mol. The high binding affinity of LPFFD is also understandable by counting the number of SC contacts. Residues L, P, F, F, and D have three, two, two, two, and three contacts, respectively, with chain VII (Figure 12). The fourth residue F from LPFFD forms one contact with chain VIII, whereas D has four contacts with chain VIII and two contacts with chain IX. In total, LPFFD has 19 SC contacts with $9\text{A}\beta_{9-40}$, where chain VII is the most susceptible to binding. One can show that KLVFF has only 13 SC contacts with the receptor (10 contacts with peptide VII and 3 contacts with chain VIII). They are formed by the four residues K, V, F, and F, as L is not bound to $9\text{A}\beta_{9-40}$ through SC contacts. Thus, as in the 2-fold-symmetric case, the binding affinity of KLVFF is lower than that of

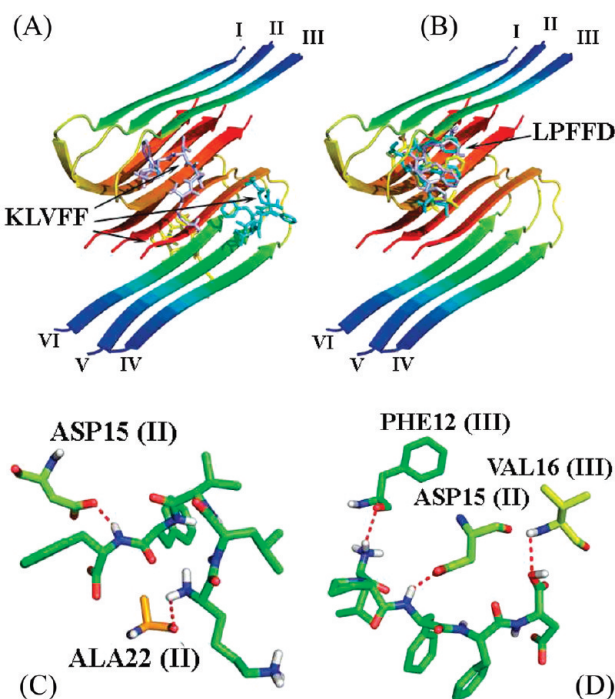


Figure 11. Binding sites of KLVFF and LPFFD to the 2-fold-symmetric $6A\beta_{9-40}$ complex (mode 1, silver; mode 2, green; mode 3, yellow) and hydrogen bonds of the best mode. KLVFF and LPFFD are on the left and right sides, respectively.

LPFFD, and one can expect that the latter degrades mature fibrils to a greater extent than the former.

Binding to 2-Fold-Symmetric 12A β_{9-40} and 3-Fold-Symmetric 18A β_{9-40} . To gain more insight into the binding of the two pentapeptides to mature fibrils, we also considered larger systems of 12 and 18 chains. In the best binding mode, the positions of KLVFF and LPFFD in complex with 12A β_{9-40} are different (Figure S11A, Supporting Information). Both peptides have 12 SC contacts with the receptor. However, their difference lies in hydrogen-bond networks (Figure S11B,C, Supporting Information). KLVFF has three HBs with chains L and J from the upper layer, whereas LPFFD is bound to the receptor through eight HBs with residues from both layers. This strong hydrogen bonding explains why LPFFD has a lower binding energy than KLVFF (Table 3).

As in $12A\beta_{9-40}$, the two peptides are also located at different places inside 3-fold-symmetric complex $18A\beta_{9-40}$ (Figure S12A, Supporting Information). However, the hydrogen bonding is notably weaker, as both peptides have only two HBs with the receptor (Figure S12B,C, Supporting Information). KLVFF is hydrogen-bonded with two chains from different patches (chain V and XVIII), whereas LPFFD is hydrogen-bonded with only one chain X. Although the two peptides have the same numbers of HBs with $18A\beta_{9-40}$, KLVFF displays a lower binding affinity (Table 3), implying that other interactions such as electrostatic and vdW interactions also make contributions. To show this, we calculated the number of SC contacts between ligand and receptor. It turns out that KLVFF has only 12 contacts (one, three, two, one, three, and two contacts with chains IV, V, VI, XV, XVI, and XVIII, respectively) against 20 contacts (one, three, two, four, four, five, and one contacts with peptides II, III, IV, V, IX, X, and XI, respectively) formed by LPFFD with

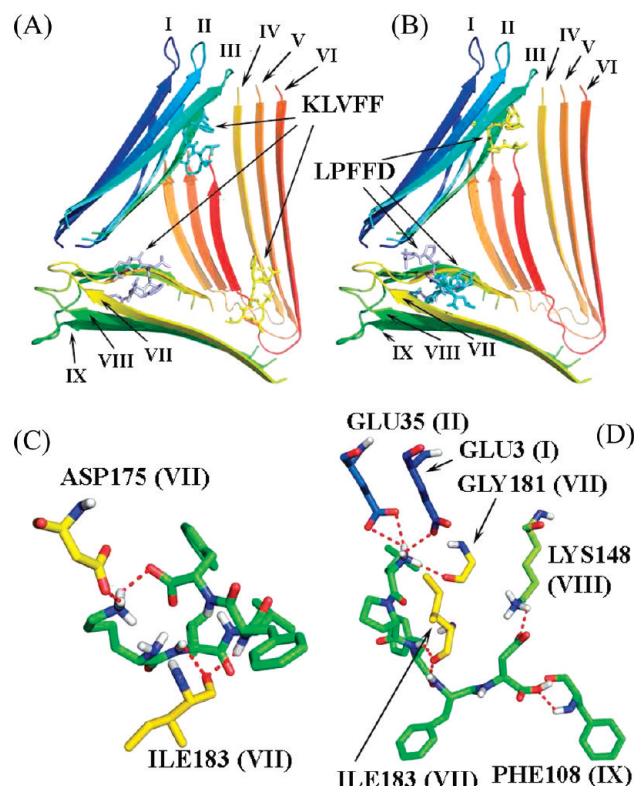


Figure 12. Binding sites of KLVFF and LPFFD to the 3-fold-symmetric $9\text{A}\beta_{9-40}$ complex (mode 1, silver; mode 2, green; mode 3, yellow) and hydrogen bonds of the best mode. KLVFF and LPFFD are on the left and right sides, respectively.

$18A\beta_{9-40}$. Thus, our results on binding energies to $12A\beta_{9-40}$ and $18A\beta_{9-40}$ further support the fact that LPFFD is bound to mature fibrils of $A\beta_{9-40}$ more tightly than KLVFF.

■ CONCLUSIONS

We have shown that LPFFD slows the oligomerization of $\text{A}\beta_{16-22}$ to a greater extent than KLVFF. The MM-PBSA calculation showed that the former has a higher binding affinity to both monomer and dimer of $\text{A}\beta_{16-22}$. Thus, for the first time, we have demonstrated theoretically that the binding ability is correlated with inhibition one.

LPFFD markedly increases the total β -content of $A\beta_{1-40}$, but it can still inhibit oligomerization because the beta enhancement takes place mainly in regions that are not prone to aggregation. This observation suggests that, in the presence of ligands, the correlation between the overall β -content, the monomer state of $A\beta$ peptides, and the aggregation rates might not hold. Instead, beta-sheet breakers interfere with oligomerization because they stabilize the monomer state of $A\beta_{1-40}$ or enlarge the gap between the native and excited states. This scenario is consistent with the hypothesis that the more stable a protein is, the slower its fibril formation will be.

If one uses the α -content as a reaction coordinate and maps the FEL onto it, then the conformational change of $\text{A}\beta_{1-40}$ obeys the weak two-state scenario. This picture becomes downhill in the presence of inhibitors. If the β -content is chosen as the reaction coordinate, then transition states do not occur in either the presence or absence of beta-sheet breakers. Thus, a single

reaction coordinate description of FEL might be not accurate enough for conformational dynamics of full-length $\text{A}\beta$ peptides.

Our canonical 300-ns MD simulations show that the most probable structure contains roughly 60%, 30%, and 10% RC, α -, and β -contents, respectively (Figure S9, Supporting Information). However, the issue of the structure of monomer $\text{A}\beta_{1-40}$ in aqueous solution remains open because of the discrepancy between the results obtained by different groups.^{42,43,82,84} The question we ask now is whether the 300-ns MD run provides useful information on the fibrilllogenesis of $\text{A}\beta_{1-40}$ and its complexes with beta-sheet breaker peptides. To clarify this problem, as a counter example, we performed additional 300-ns MD simulations for monomer $\text{A}\beta_{1-42}$ under the same conditions as in the case of $\text{A}\beta_{1-40}$. The time dependence of the β -content of both full-length peptides is shown in Figure S13 (Supporting Information). Clearly, in accord with prior simulations,^{42,43} $\text{A}\beta_{1-42}$ displays a higher percent of beta structure compared to $\text{A}\beta_{1-40}$. In other words, the 300-ns MD simulations correctly capture the fact that the higher propensity for aggregation of the former is associated with a higher β -content in the monomer state. Thus, our canonical simulations probably mimic the effect of pentapeptides on the secondary structure of $\text{A}\beta_{1-40}$.

To further support the fact that our canonical 300-ns MD simulations of $\text{A}\beta_{1-40}$ produce structures relevant to experimental ones, we used chemical shifts predicted from our simulations δ_{sim} and determined experimentally. The δ_{sim} values were computed using the SHIFT program^{88,89} and conformational ensemble collected at equilibrium. Our in silico result obtained for C_α atoms is highly correlated (correlation level $R = 0.95$) with the solid-state NMR experiments of Petkova et al.³ (Figure S14, Supporting Information). A high correlation was also observed for atoms N_α (results not shown). Therefore, the strong correlation between our theoretical data and those produced experimentally indicates that our 300-ns MD simulations produce the $\text{A}\beta_{1-40}$ ensemble reasonably well.

Having used the MM-PBSA and docking methods, we showed that KLVFF is more weakly bound to $\text{A}\beta_{1-40}$ and its mature fibrils in comparison with LPFFD. One of the possible implications of this result is that the latter degrades $\text{A}\beta$ fibrils more strongly than the former. It would be interesting to check this prediction experimentally.

■ ASSOCIATED CONTENT

S Supporting Information. MM-PBSA method and Figures S1–S14. This material is available free of charge via the Internet at <http://pubs.acs.org>.

■ AUTHOR INFORMATION

Corresponding Author

*E-mail: masli@ifpan.edu.pl.

■ ACKNOWLEDGMENT

This work was supported by the Ministry of Science and Informatics in Poland (Grant 202-204-234) and the Department of Science and Technology at Ho Chi Minh city, Vietnam. We are very thankful to R. Tycko for providing us with structures of $\text{A}\beta_{9-40}$ fibrils.

■ REFERENCES

- (1) Eanes, E. D.; Glenner, G. G. *J. Histochem. Cytochem.* **1968**, *16*, 673–677.
- (2) Kirschner, D. A.; Abraham, C.; Selkoe, D. J. *Proc. Natl. Acad. Sci. U.S.A.* **1986**, *83*, 503–507.
- (3) Petkova, A. T.; Ishii, Y.; Balbach, J.; Antzutkin, O.; Leapman, R.; Delaglio, F.; Tycko, R. *Proc. Natl. Acad. Sci. U.S.A.* **2002**, *99*, 16742–16747.
- (4) Luhrs, T.; Ritter, C.; Adrian, M.; Riek-Lohr, D.; Bohrmann, B.; Doeli, H.; Schubert, D.; Riek, R. *Proc. Natl. Acad. Sci. U.S.A.* **2005**, *102*, 17342–17347.
- (5) Hardy, J.; Selkoe, D. J. *Science* **2002**, *297*, 353–356.
- (6) Kayed, R.; Head, E.; Thompson, J. L.; McIntire, T. M.; Milton, S. C.; Cotman, C. W.; Glabe, C. G. *Science* **2003**, *300*, 486–489.
- (7) Caughey, B.; Lansbury, P. T. *Annu. Rev. Neurosci.* **2003**, *26*, 267–298.
- (8) Svennerholm, L. *Life Sci.* **1994**, *55*, 2125–2134.
- (9) Castillo, G. M.; Ngo, C.; Cummings, J.; Wight, T. N.; Snow, A. D. *J. Neurochem.* **1997**, *69*, 2452–2465.
- (10) Yatin, S. M.; Yatin, M.; Varadarajan, S.; KB, K. B. A.; Butterfield, D. A. *J. Neurosci. Res.* **2001**, *63*, 395–401.
- (11) Dolphin, G. T.; Chierici, S.; Ouberai, M.; Dumy, P.; Garcia, J. *ChemBioChem* **2008**, *9*, 952–963.
- (12) Evans, C. G.; Wisen, S.; Gestwicki, J. E.; Jason, E. *J. Biol. Chem.* **2006**, *281*, 33182–33191.
- (13) Bush, A. I. *Neurobiol. Aging* **2002**, *23*, 1031–1038.
- (14) Nitz, M.; Fenili, D.; Darabie, A. A.; Wu, L.; Cousins, J. E.; McLaurin, J. *FEBS J.* **2008**, *275*, 1663–1674.
- (15) Takahashi, T.; Tada, K.; Mihara, H. *Mol. Biosyst.* **2009**, *5*, 986–991.
- (16) Hawkes, C. A.; Ng, V.; MacLaurin, J. *Drug Dev. Res.* **2009**, *70*, 111–124.
- (17) Yamin, G.; Ono, K.; Inayathullah, M.; Teplow, D. B. *Curr. Pharm. Des.* **2008**, *14*, 3231–3246.
- (18) Williams, P.; Sorribas, A.; Howes, M. J. R. *Nat. Prod. Rep.* **2011**, *28*, 48–77.
- (19) Howes, M. J. R.; Houghton, P. J. *Pharmacol., Biochem. Behav.* **2003**, *75*, 513–527.
- (20) Hughes, E.; Burke, R. M.; Doig, A. J. *J. Biol. Chem.* **2000**, *275*, 25109–25115.
- (21) Gordon, D. J.; Tappe, R.; Meredith, S. C. *J. Pept. Res.* **2002**, *60*, 37–55.
- (22) Chebaro, Y.; Derreumaux, P. *Proteins: Struct., Funct., Genet.* **2009**, *75*, 442–452.
- (23) Soto, P.; Griffin, M. A.; Shea, J. E. *Biophys. J.* **2007**, *93*, 3015–3025.
- (24) Tjernberg, L. O.; Naslund, J.; Lindqvist, F.; Jahansson, J.; Karlstrom, A. R.; Thyberg, J.; Terenius, L.; Nordstedt, C. *J. Biol. Chem.* **1996**, *271*, 8545–8548.
- (25) Soto, C. M.; Kindy, S.; Baumann, M.; Frangione, B. *Biochem. Biophys. Res. Commun.* **1996**, *226*, 672–680.
- (26) Adessi, C.; Soto, C. *Drug Dev. Res.* **2002**, *56*, 184–193.
- (27) Li, H. Y.; Monien, M. B.; Lomakin, A.; Zemel, R.; Fradinger, E. A.; Tan, M. A.; Spring, S. M.; Urbanc, B.; Xie, C. W.; Benedek, G. B.; Bitan, G. *Biochemistry* **2010**, *49*, 6358–6364.
- (28) Li, H. Y.; Monien, M. B.; Urbanc, E. A. F. B.; Bitan, G. *Biochemistry* **2010**, *49*, 1259–1267.
- (29) Wu, C.; Murray, M. M.; Summer, S. L. B. L.; Condron, M. M.; Bitan, G.; Shea, J. E.; Bowers, M. T. *J. Mol. Biol.* **2009**, *387*, 492–501.
- (30) Soto, C.; Sigurdsson, E. M.; L, L. M.; Kumar, R. A.; Castano, E. M.; Frangione, B. *Nat. Med.* **1998**, *4*, 822–826.
- (31) Yang, C.; Zhu, X. L.; Li, J. Y.; Shi, R. W. *J. Mol. Model.* **2010**, *16*, 813–821.
- (32) Hess, B.; Kutzner, C.; van der Spoel, D.; Lindahl, E. *J. Chem. Theory Comput.* **2008**, *4*, 435–447.
- (33) Tarus, B.; Straub, J. E.; Thirumalai, D. *J. Am. Chem. Soc.* **2006**, *128*, 16159–16168.
- (34) Sciarretta, K. L.; Gordon, D. J.; Petkova, A. T.; Tycko, R.; Meredith, S. C. *Biochemistry* **2005**, *44*, 6003–6014.

- (35) Chang, W. L. E.; Takeda, T.; Raman, E. P.; Klimov, D. K. *Biophys. J.* **2010**, *98*, 2662–2670.
- (36) Pallitto, M. M.; Ghanta, J.; Heizelman, P.; Kiessling, L. L.; Murphy, R. M. *Biochemistry* **1999**, *38*, 3570–3578.
- (37) Srinivasan, J.; T., E. C., III; Cieplak, P.; Kollman, P. A.; Case, D. A. *J. Am. Chem. Soc.* **1998**, *120*, 9401–9409.
- (38) Kollman, P. A.; Massova, I.; Reyes, C.; Kuhn, B.; Huo, S. H.; Chong, L.; Lee, M.; Lee, T.; Duan, Y.; Wang, W.; Donini, O.; Cieplak, P.; Srinivasan, J.; Case, D. A.; Cheatham, T. E. *Acc. Chem. Res.* **2000**, *33*, 889–897.
- (39) Jarrett, J. T.; Berger, E. P.; Lansbury, P. T. *Biochemistry* **1993**, *32*, 6493–6497.
- (40) Lomakin, A.; Chung, D. S.; Benedek, G. B.; Kirschner, D. A.; Teplow, D. B. *Proc. Natl. Acad. Sci. U.S.A.* **1996**, *93*, 1125–1129.
- (41) Lomakin, A.; Teplow, D. B.; Kirschner, D. A.; Benedek, G. B.; Teplow, D. B. *Proc. Natl. Acad. Sci. U.S.A.* **1997**, *93*, 7942–7947.
- (42) Sgourakis, N. G.; Yan, Y. L.; McCallum, S. A.; Wang, C. Y.; Garcia, A. E. *J. Mol. Biol.* **2007**, *368*, 1448–1457.
- (43) Yang, M.; Teplow, D. B. *J. Mol. Biol.* **2008**, *384*, 450–464.
- (44) Paravastu, A. K.; Leapman, R. D.; Yau, W. M.; Tycko, R. *Proc. Natl. Acad. Sci. U.S.A.* **2008**, *105*, 18349–18354.
- (45) Sanner, M. F. *J. Mol. Graphics Mod.* **1999**, *17*, 57–61.
- (46) Watson, A. A.; Fairlie, D. P.; Craik, D. J. *Biochemistry* **1998**, *37*, 12700–12706.
- (47) Sticht, H.; Bayer, P.; Willbold, D.; Dames, S.; Hilbich, C.; Beyreuther, K.; Frank, R. W.; Rosch, P. *Eur. J. Biochem.* **1995**, *233*, 293–298.
- (48) Coles, M.; Bicknell, W.; Watson, A. A.; Fairlie, D. P.; Craik, D. J. *Biochemistry* **1998**, *37*, 11064–11077.
- (49) Lee, J. P.; Stimson, R. R.; Ghilardi, J. R.; Mantyh, P. W.; Lu, Y.-A.; Felix, A. M.; Llanos, W.; Behbin, A.; Cummings, M.; Van Criekinge, M.; Timms, W.; Maggio, J. E. *Biochemistry* **1995**, *34*, 5191–5200.
- (50) Petkova, A. T.; Yau, W. M.; Tycko, R. *Biochemistry* **2006**, *45*, 498–512.
- (51) Trott, O.; Olson, A. J. *J. Comput. Chem.* **2010**, *31*, 455–461.
- (52) Morris, G. M.; Godsell, D. S.; Halliday, R. S.; Huey, R.; Hart, W. E.; Belew, R. K.; Olson, A. J. *J. Comput. Chem.* **1998**, *19*, 1639–1662.
- (53) Morris, G. M.; Godsell, D. S.; Huey, R.; Olson, A. J. *J. Comput.-Aided Mol. Des.* **1998**, *10*, 293–304.
- (54) Shanno, D. F. *Math. Comput.* **1970**, *24*, 647–656.
- (55) van Gunsteren, W.; Billeter, S. R.; Eising, A. A.; Hünenberger, P. H.; Krüger, P.; Mark, A. E.; Scott, W.; Tironi, I. *Biomolecular Simulation: The GROMOS96 Manual and User Guide*; vdf Hochschulverlag AG an der ETH: Zürich, Switzerland, 1996.
- (56) Berendsen, H. J. C.; Postma, J.; van Gunsteren, W.; Hermans, J. *Intermolecular Forces*; Reidel: Dordrecht, The Netherlands, 1996.
- (57) Nguyen, P. H.; Li, M. S.; Stock, G.; Straub, J. E.; Thirumalai, D. *Proc. Natl. Acad. Sci. U.S.A.* **2007**, *104*, 111–116.
- (58) Nam, H. B.; Kouza, M.; Zung, H.; Li, M. S. *J. Chem. Phys.* **2010**, *132*, 165104.
- (59) Hockney, R. W.; Goel, S. P.; Eastwood, J. *J. Comput. Phys.* **1974**, *14*, 148–158.
- (60) Hess, B.; Bekker, H.; Berendsen, H. J. C.; Fraaije, J. G. E. M. *J. Comput. Chem.* **1997**, *18*, 1463–1472.
- (61) Bussi, G.; Donadio, D.; Parrinello, M. *J. Chem. Phys.* **2007**, *126*, 014101.
- (62) Berendsen, H. J. C.; Postma, J. P. M.; Vangunsteren, W. F.; Dinola, A.; Haak, J. R. *J. Chem. Phys.* **1984**, *81*, 1463–1472.
- (63) Darden, T.; York, D.; Pedersen, L. *J. Chem. Phys.* **1993**, *98*, 10089–10092.
- (64) Cecchini, M.; Rao, F.; Seeber, M.; Caflisch, A. *J. Chem. Phys.* **2004**, *121*, 10748–10756.
- (65) Klimov, D. K.; Thirumalai, D. *Structure* **2003**, *11*, 295–307.
- (66) Munoz, V.; Serrano, L. *Proteins: Struct., Funct., Genet.* **1994**, *20*, 301–311.
- (67) Frishman, D.; Argos, P. *Proteins: Struct., Funct., Genet.* **1995**, *23*, 566–579.
- (68) Heinig, M.; Frishman, D. *Nucleic Acids Res.* **2004**, *32*, W500–2.
- (69) Ono, K.; Condron, M. M.; Ho, L.; Wang, J.; Zhao, W.; Pasinetti, G. M.; Teplow, D. B. *J. Biol. Chem.* **2008**, *283*, 32176–32187.
- (70) Yang, F. S.; Lim, G. P.; Begum, A. N.; Ubeda, O. J.; Simmons, M. R.; Ambegaokar, S. S.; Chen, P. P.; Kayed, R.; Glabe, C. G.; Frautschi, S. A.; Cole, G. M. *J. Biol. Chem.* **2005**, *280*, 5892–5901.
- (71) Chiti, F.; Stefani, M.; Taddei, N.; Ramponi, G.; CM, C. M. D. *Nature* **2003**, *424*, 805–808.
- (72) Amaro, R. E.; Baron, R.; McCammon, J. A. *J. Comput.-Aided Mol. Des.* **2007**, *22*, 693–705.
- (73) Lu, H.; Schulten, K. *Biophys. J.* **2000**, *79*, 51–65.
- (74) Takeda, T.; Klimov, D. K. *J. Phys. Chem. B* **2009**, *113*, 6692–6702.
- (75) Lee, J. P.; Stimson, E. R.; Ghilardi, J. R.; Mantyh, P. W.; Lu, Y. A.; Felix, A. M.; Llanos, W.; Benhin, A.; Cummings, M.; Timms, W.; Maggio, J. E. *Biochemistry* **1995**, *34*, 5191–51200.
- (76) Lazo, N. D.; Grant, M. A.; Condrone, M. C.; Rigby, A. C.; Teplow, D. B. *Protein Sci.* **2005**, *14*, 1581–1596.
- (77) Shao, H. Y.; Jao, S. C.; Ma, K.; Zagorski, M. G. *J. Mol. Biol.* **1999**, *285*, 755–773.
- (78) Barrow, C. J.; Yasuda, A.; Kenny, P. T. M.; Zagorski, M. G. *J. Mol. Biol.* **1992**, *225*, 1075–1093.
- (79) Sticht, H.; Bayer, P.; Willbold, D.; Dames, S.; Hilbich, C.; Beyreuther, K.; Frank, R. W.; Rosch, P. *Eur. J. Biochem.* **1995**, *233*, 293–298.
- (80) Tomaselli, S.; Esposito, V.; Vangone, P.; van Nuland, N. A.; Bonvin, A. M.; Guerrini, R.; Tancredi, T.; Temussi, P. A.; Picone, D. *ChemBioChem* **2006**, *7*, 257–267.
- (81) Crescenzi, O.; Tomaselli, S.; Guerrini, R.; Salvadori, S.; D'Ursi, A. M.; Temussi, P. A.; D, D. P. *Eur. J. Biochem.* **2002**, *269*, 5642–5648.
- (82) Vitalis, A.; Caflisch, A. *J. Mol. Biol.* **2010**, *403*, 148–165.
- (83) Fezoui, Y.; Teplow, D. B. *J. Biol. Chem.* **2002**, *277*, 36948–36954.
- (84) Rojas, A.; Liwo, A.; Browne, D.; Scheraga, H. A. *J. Mol. Biol.* **2010**, *404*, 537–552.
- (85) Li, M. S.; Co, N. T.; Hu, C. K.; Straub, J. E.; Thirumalai, D. *Phys. Rev. Lett.* **2010**, *105*, 218101.
- (86) Reddy, G.; Straub, J. E.; Thirumalai, D. *J. Phys. Chem. B* **2009**, *113*, 1162–1172.
- (87) Wood, S. J.; Wetzel, R.; Martin, J. D.; Hurle, M. R. *Biochemistry* **1995**, *34*, 724–730.
- (88) Xu, X. P.; Case, D. A. *J. Biomol. NMR* **2001**, *21*, 321–333.
- (89) Xu, X. P.; Case, D. A. *Biopolymers* **2002**, *65*, 408–423.